DEVELOPMENT OF A NEW METHOD TO CALCULATE INCIDENT RADIANT HEAT FLUX FROM FIRE USING PLATE THERMOMETER

By

QINGTONG LIU

Bachelor of Science in Fire Protection and Safety Technology

Oklahoma State University

Stillwater, Oklahoma

2017

Submitted to the Faculty of the
Graduate College of the
Oklahoma State University
in partial fulfillment of
the requirements for
the Degree of
MASTER OF SCIENCE
May, 2019

DEVELOPMENT OF A NEW METHOD TO

CALCULATE INCIDENT RADIANT HEAT FLUX

FROM FIRE USING PLATE THERMOMETER

Thesis Approved:

Dr. Haejun Park

Thesis Adviser

Dr. Bryan Hoskins

Committee Member

Dr. Yu Feng

Committee Member

ACKNOWLEDGEMENTS

Firstly, I would like to thank my thesis advisor Dr. Haejun Park of Fire Protection and Safety Technology at Oklahoma State University for the continued support and guidance in all the time of research. The door to Dr. Park office was always open whenever I ran into a trouble or had a question about my research. I would also like to thank Dr. Bryan Hoskins and Dr. Yu Feng for their valuable thoughts and comments, which helped me to complete the thesis. I would also like to thank all the professors in the Fire Protection and Safety Technology major for their participation and input. My sincere thanks also goes to Dr. Qingsheng Wang of Chemical Engineering at Texas A&M, who gave me valuable suggestion on the research.

Last but not least, I must express my very profound gratitude to my parents for providing me with unfailing support. Most importantly, I wish to thank to my supportive and smart husband, Ruiqing Shen, who provide unending inspiration of research. This thesis would not have been possible without their warm love, continued patience. Thank you!

Name: QINGTONG LIU

Date of Degree: MAY, 2019

Title of Study: DEVELOPMENT OF A NEW METHOD TO CALCULATE INCIDENT RADIANT HEAT FLUX FROM FIRE USING PLATE THERMOMETER

Major Field: FIRE SAFETY AND EXPLOSION PROTECTION

Abstract: A plate thermometer (PT) that consists of a thin Inconel plate with the substrate of one layer of 6.4 mm thick and another layer of 12.7 mm thick ceramic fiber boards, was developed to calculate the incident radiant heat flux and equivalent total heat flux. However, by simply assuming 1-D heat transfer within PT, the equivalent total heat flux directly calculated using PT is lower than the reading of commercially available total heat flux gauge due to some uncertainties, such as emissivity, the error of temperature measurement, the lateral heat loss, the thermo-physical properties, and so on. In this study, with the calibration conducted under a cone calorimeter heater, two new methods of considering the uncertainties above were proposed, by introducing a new concept of ideal surface temperature of PT in an ideal 1-D heat transfer model or perfect insulation model, respectively. The calculated equivalent total heat flux using PT was compared to the reading of a commercially available Schmidt-Boelter type water-cooled total heat flux gauge for validation in a controlled thermal exposure scenario and a real fire scenario. With the method of employing the ideal surface temperature of PT in an ideal 1-D heat transfer model, the results showed very good agreement not only in the controlled thermal exposure from the cone calorimeter heater, but also in the real fire scenario. In spite of some discrepancy, due to its simplicity, directly employing the ideal surface temperature of PT in a perfect insulation model is still a useful method for fire engineers to characterize the changing trend and level of the equivalent total heat flux in the fire test field.

TABLE OF CONTENTS

Chapter Page

LIST OF TABLES

Table Page

LIST OF FIGURES

Figure Page

NOMENCLATURE

c_p	Specific heat of Inconel 600 metal plate [kJ/(kg K)]
c_{ins}	Specific heat of insulation [kJ/(kg K)]
c_{met}	Specific heat of metal plate [kJ/(kg K)]
C	Thin skin calorimeter correction factor
C_{PT}	Heat storage lumped heat capacity [J/(m^2 K)]
d_{ins}	Thickness of insulation (m)
d_{met}	Thickness of metal plate (m)
h	Convective heat transfer coefficient (W/m^2 K)
h_{cont}	Contact correction factor (W/m^2 K)
k	Thermal conductivity (W/m °C)
K_{cond}	Conduction correction factor (W/m^2 K)
L	Length (m)
$\overline{Nu}$	Nusselt number
Pr	Prandtl number
$\dot{q}''_{cond}$	Conduction loss (W/m^2)
$\dot{q}''_{cont}$	Contact heat loss (W/m^2)
$\dot{q}''_{conv}$	Convective heat flux (W/m^2)
$\dot{q}''_{HFG}$	Total heat flux of Schmidt-bolter type total flux gauge (W/m^2)
$\dot{q}''_{inc}$	Incident heat flux (W/m^2)
$\dot{q}''_{inc-rad}$	Incident radiation heat flux (W/m^2)
$\dot{q}''_{rad-in}$	Radiation heat flux into PT (W/m^2)
$\dot{q}''_{re-rad}$	Re-radiation (W/m^2)
$\dot{q}''_{stored}$	Heat energy stored (W/m^2)
Ra	Rayleigh number
T_{amb}	Ambient temperature (K)
T_∞	Ambient temperature (K)
T_g	Gas temperature (K)
T_{PT}	Temperature of metal plate (K)
T_s	Measured surface temperature of Inconel 600 metal plate (K)

$T_{s-ideal}$	Ideal surface temperature of Inconel 600 metal plate (K)
T_0	Temperature of the first node of ceramic fiber board (K)
t	Time (s)
β	Portion of the insulation
ε_{HFG}	Surface emissivity of Schmidt-bolter type total heat flux gauge
ε_{PT}	Surface emissivity of PT
α_{disc}	Absorptivity of the thin skin calorimeter metallic disc
ρ	Density of Inconel 600 metal plate (kg/m^3)
ρ_{ins}	Density of insulation (kg/m^3)
ρ_{met}	Density of metal plate (kg/m^3)
σ	Stefan-Boltzmann constant [$W/(m^2 K^4)$]
δ	Thickness of Inconel 600 metal plate (m)

CHAPTER I

INTRODUCTION

The heat transfer from a fire and other external heat sources to its surrounding environment and adjacent surfaces, significantly affects the strength and performance of building elements in compartment fires, such as load-bearing elements, fire barrier, and fire resistance door [1], [2]. Additionally, that heat transfer is also a key factor associated with the ignition of combustible materials, flame spread over solid surfaces, and the growth and spread of wildland fire. In order to determine the thermal interaction between the heat sources and the surrounding in a fire, it is of essence to accurately measure the amount of heat flux that the surface of interest is exposed to.

In practice, the commercially available water-cooled Schmidt-Boelter gauge and Gardon gauge are widely used in fire tests to measure total heat flux because of their fast thermal response and rigorous and accurate calibration procedure in a well-defined thermal environment [3]. For this type of heat flux sensor, water cooling is often required to maintain the temperature of the gauge exposed surface at acceptable levels, what is usually near ambient temperature. Nevertheless, the water cooling effect is also attributed to condensation and soot deposition on these gauge surface, which at least to some degree, affects their accuracy in real fire scenarios [4]. Additionally, they are not convenient to be employed in the field where a reliable water supply is not always available, like fire tests in tunnels or wildland.

Plate Thermometer (PT) is a technically simple but physically robust instrument. In recent years, some researchers [5], [6] have endeavored to use Plate Thermometer (PT) or Thin Skin

Calorimeter (TSC) [7], [8] to measure heat flux [9], [10], as an alternative or a complement to commercially available water-cooled heat flux gauges, especially in conditions without the need of water supply, although the PT was initially developed for monitoring the effective temperature of specimens in fire resistance furnace tests [11]. So far PT has been applied in tests in pool fire, compartment fire, and wildland fire. However, it is found that if PT is exposed to incident radiation heat flux of high intensity in an ambient surrounding gas temperature condition, the calculated incident radiation heat flux using PT is somewhat lower than the actual incident radiation heat flux [9]. Various methods have been developed to improve the accuracy of the calculated heat flux using PT in an ambient surrounding gas temperature condition, but these methods are mainly originated to correct the thermal energy balance equation of PT. Considering the fact that a lot of uncertain factors exist to affect the temperature reading of PT, like heat loss, thermocouple welding, thermocouple wire heat conduction, etc., a new concept of ideal surface temperature of PT is defined in this study to correct the actual temperature reading of PT. Based on this new concept, two new calculation methods are proposed to improve the accuracy of heat flux measurement using PT, particularly in an ambient surrounding gas temperature condition.

CHAPTER II

BACKGROUND

2.1 General heat transfer

This section describes the general heat transfer theory in thermal engineering. Basically, heat transfer is defined as 'thermal energy in transit due to a spatial temperature difference' and it is an area of thermal engineering that focuses on heat transport, exchange, and redistribution. Heat transfer occurs when the temperature is different within a medium or between media. Heat transfer processes are divided into three modes, which are conduction, convection, and radiation. Conduction and radiation heat transfer are energy transfer modes. Conduction heat transfer occurs when a temperature gradient exists in a medium. Based on the Fourier's Law of conduction, the general conduction heat transfer can be expressed in proportion to the temperature differences across the body and the distance. For one dimensional, the equation is expressed as Eq. (1)

$$q''_x = -k\frac{dT}{dx} \tag{1}$$

Where:

q''_x = Heat transfer rate (W/m^2)

k = Thermal conductivity (W/m K)

T = Temperature (K)

x = Distance (m)

Convection heat transfer is the mode of heat transfer about a solid involving movement of a surrounding environment. The convection heat transfer is divided into two modes, which are natural convection and forced convection caused by external means. Generally, the convection heat transfer can be expressed as Eq. (2)

$$\dot{q}''_{conv} = h(T_s - T_\infty) \tag{2}$$

Where,

$\dot{q}''_{conv}$ = Convection heat transfer (W/m^2)

h = Convection heat transfer coefficient (W/m^2 K)

T_s = Surface temperature (K)

T_∞ = Ambient temperature (K)

The dominant mode of heat transfer in the most of real fire scenarios is thermal radiation. It occurs by the mechanism of photon emission or electromagnetic wave emission. Based on the Stefan-Boltzmann law, the radiation heat transfer can be expressed as Eq. (3)

$$\dot{q}''_{rad} = \varepsilon\sigma T_s^4 \tag{3}$$

Where:

$\dot{q}''_{rad}$ = Radiation heat transfer

ε =Emissivity

σ = Stefan-Boltzmann constant : $5.67 \times 10^{-8} W / m^2 \bullet K^4$

2.2 Schmidt-Boelter type water-cooled heat flux gauge

Basically, the Schmidt-Boelter type water-cooled heat flux gauge and radiometer are commercially heat flux measurement tool and they are shown in Figure 1. They are an internal thermopile sensor, which generates a voltage output signal based on the temperature difference within the reference material. The Schmidt-Boelter type water-cooled heat flux gauge measures the radiation heat flux and convection heat flux. The maximum value of its measurement is 200 kW/ m^2. However, the Schmidt-Boelter type water-cooled radiometer measures the radiation heat flux only. The convection heat flux is blocked by the sapphire window. The voltage output signal is directly proportional to the heat flux incident upon the sensing surface of Schmidt-Boelter type water-cooled heat flux gauge and radiometer. The relationship between the voltage output signal and the heat flux is obtained on the basis of the calibration results [12]. The calibration method of the Schmidt-Boelter type water-cooled total heat flux gauge (THG) is standardized and its application to measure total heat flux is approved in fire experiments. Therefore, it is selected as the reference value in this study.

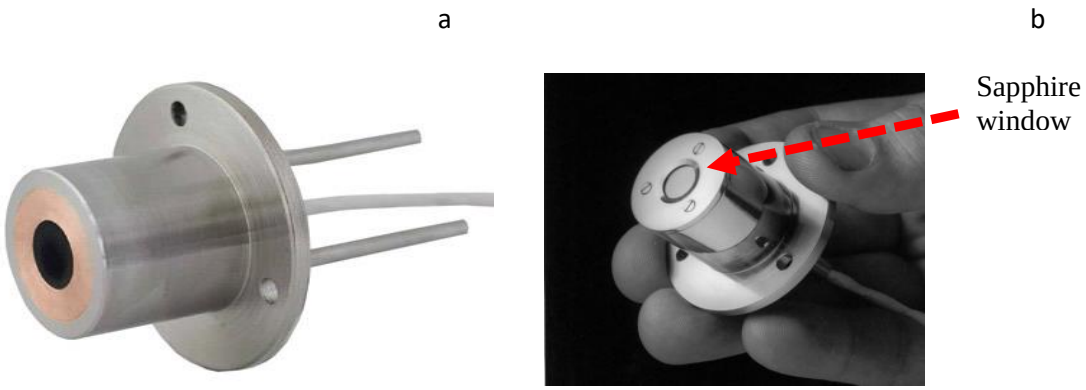

Figure 1. (a) Schmidt-Boelter type water-cooled heat flux gauge; (b) Radiometer.

In the mixed radiation/convection environment, the total heat flux ($\dot{q}''_{HFG}$) measured by THG is classically expressed as Eq. (4)

$$\dot{q}''_{HFG} = \varepsilon_{HFG}\dot{q}''_{inc-rad} + h\,(T_g - T_\infty) - \varepsilon_{HFG}\sigma T_\infty^{\,4} \quad (4)$$

Where:

$\dot{q}''_{HFG}$ = Total heat flux of Schmidt-bolter type total flux gauge (W/m^2)

ε_{HFG} = Surface emissivity of Schmidt-bolter type total heat flux gauge

$\dot{q}''_{inc-rad}$ = Incident radiation heat flux (W/m^2)

T_g = Gas temperature (K)

σ = Stefan-Boltzmann constant [W/(m^2 K^4)]

The total heat flux ($\dot{q}''_{HFG}$) is the sum of the net heat flux contributed by radiation and convection. To maximum the amount of absorbed incident radiation heat flux, the exposed surface of THG is coated with high emissivity black paint. Based on the description of the User Manual SBG01, the emissivity of THG is as high as 0.95 [12]. In this expression, it is noted that the absorptivity is assumed to be equal with the emissivity of the front surface. Due to the water cooling effect to the front surface of THG, the temperature of the front surface is near the ambient temperature (T_∞) in a range of 20-80 °C. In this case, because of the large temperature difference between the fluid in the vicinity and the front surface of THG, the contribution by convective heat transfer is maximized as well. Nevertheless, with its low temperature, the amount of re-radiation heat flux from the front surface of THG is minimized. Given the low value of T_∞, the amount of re-radiation heat flux is very small, which has less contribution of heat loss in Eq. (4) and has been neglected by some

researchers [2]. Therefore, what THG measures is the maximum total heat flux that a surface can be exposed to, which some researchers are referred to as cold surface heat flux.

If THG is used in an ambient surrounding gas temperature condition, due to the negligible temperature difference between the front surface and the surrounding gas temperature, the convection term in Eq. (4) can be ignored. In this case, the heat balance on the surface of THG is written as Eq. (5).

$$\dot{q}''_{HFG} = \varepsilon_{HFG}\dot{q}''_{inc-rad} - \varepsilon_{HFG}\sigma T_{\infty}^{4} \quad (5)$$

There are some advantages of Schmidt-Boelter type water-cooled heat flux gauge and radiometer. First, they were proven in thousands of applications for over thirty years. Second, they have high accuracy measurement results and fast thermal response. However, they also have some disadvantages, especially using in the real fire scenario. The most disadvantage is the requirement of water supply. The water supply is not always available in a real environment, as well as the distance between gauge and water supply is limitative. It is also regarded as an expensive tool compared to plate thermometer (PT). The advantages of the new PT may include a low manufacturing cost, consistent measurement performance in exceedingly harsh conditions such as within fire, convenient usage without a water supply which is not always available in the real environment.

2.3 Plate Thermometer (PT) in standards

The standards (ISO 834 and EN1363-1) specify that the PT consists of a 0.7-mm-thick nickel alloy plate with a size of 100 mm×100 mm, a shielded thermocouple (TC) (typically Type K) welded to the geometric center of the unexposed surface of nickel alloy plate, and a 10-mm-thick inorganic insulation material attached to the backside of nickel alloy plate [13], [14]. This TC reads the exposed surface temperature of PT based on lumped heat capacity analysis. The lumped heat capacitance analysis is required to check if the temperature differences across the body are

relatively small. The PT in standards is assumed in a perfect insulation condition, in terms of the heat loss between the metal plate and the back-insulation pad being negligible, especially when being exposed to a thermal environment with high gas temperature and high level of radiation heat flux, like inside a fire resistance test furnace. Therefore, taking the nickel alloy plate as the control volume, the heat energy balance of PT in standards can be schematically expressed in Figure 2 and formulated in Eq. (6) when the PT is exposed to a mixed radiation/convection condition.

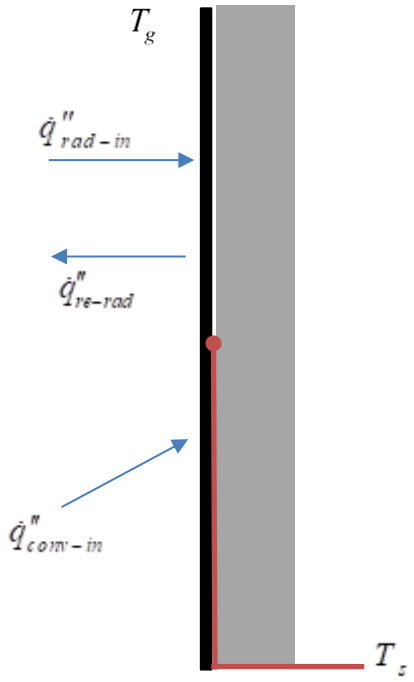

Figure 2. Energy balance of PT in a mixed radiation/convection conditions.

$$\dot{q}''_{stored} = \dot{q}''_{rad-in} + \dot{q}''_{conv} - \dot{q}''_{re-rad} \quad (6)$$

Where:

$\dot{q}''_{stored}$ = Heat energy stored (W/m^2)

$\dot{q}''_{rad-in}$ = Radiation heat flux into PT (W/m^2)

$\dot{q}''_{conv}$ = Convective heat flux (W/m^2)

$\dot{q}''_{re-rad}$ = Re-radiation (W/m^2)

Given the physical meaning of each term in Eq. (6), the expanded equation of Eq. (6) can be expressed as Eq (7).

$$\rho c_p \delta \frac{dT_s}{dt} = \varepsilon_{PT} \dot{q}''_{inc-rad} + h\ (T_g - T_s) - \varepsilon_{PT} \sigma T_s^4 \tag{7}$$

Where:

ρ = Density of Inconel 600 metal plate (kg/m^3)

c_p = Specific heat of Inconel 600 metal plate [kJ/(kg K)]

δ = Thickness of Inconel 600 metal plate (m)

T_s = Measured surface temperature of Inconel 600 metal plate (K)

t = Time (s)

ε_{PT} = Surface emissivity of PT

Rearranging the terms above, the incident radiation heat flux can then be calculated as shown in Eq. (8) based on the measured surface temperature of PT (T_s), gas temperature, convective heat transfer coefficient, and the thermo-physical properties of nickel alloy plate of PT.

$$\dot{q}''_{inc-rad} = \frac{1}{\varepsilon_{PT}} \rho c_p \delta \frac{dT_s}{dt} - \frac{1}{\varepsilon_{PT}} h\ (T_g - T_s) + \sigma T_s^4 \tag{8}$$

The PT in standards has been used to measure incident radiation heat flux in the real fire scenarios. It is found that the calculation method of incident radiation heat flux of PT above performs well for the situation where the temperature difference between the metal plate and the back insulation pad is very small, like in a fire resistance furnace or in a steady state [10]. However, the calculated incident radiation heat flux using PT is significantly lower than that measured by THG, especially during the heating phase when the temperature difference between the metal plate and the back insulation pad is large. In an ambient surrounding gas temperature condition, this underestimation

is more noticeable. This is because, in fact, the amount of heat loss may not be negligible in such a scenario. In addition, it is found that the heat loss includes not only the amount of heat loss from the metal plate to insulation pad and the surroundings but also from the thermocouple welding point of the metal plate to the edges [10]. Moreover, the measurement error of temperature using TC and the uncertainty associated with the emissivity of the exposed surface of nickel alloy plate also kind of contributes to the underestimation of incident radiation heat flux measured using PT. Therefore, due to the fact that the heat loss is a nonnegligible term in the calculation of incident radiation heat flux, various methods were developed to consider the amount of heat loss in order to improve the accuracy of PT measurement [5], [9], [10]. The following are some examples reported in the literature regarding heat loss calculation.

2.4 Literature review on heat loss

2.4.1 Ingason's method

Ingason et al. [10] assumed that the heat loss term is a combination of the heat loss caused by two-dimensional conduction within the metal plate from the thermocouple welding point in the center to the metal plate edges, and heat loss by conduction through the insulation to the back side of the PT. In order to improve the accuracy of measured incident radiation heat flux using PT, a correction factor, $\dot{q}''_{cond}$, was used to account for the heat loss through the insulation to the back of PT when the surrounding air is at ambient temperature, and it is defined as

$$\dot{q}''_{cond} = K_{cond}(T_s - T_{amb}) \tag{9}$$

Where:

$\dot{q}''_{cond}$ = Conduction loss (W/m^2)

K_{cond} = Conduction correction factor (W/m^2 K)

T_{amb} = Ambient temperature (K)

This term is a product of a conduction correction factor (K_{cond}) and the temperature difference between the nickel alloy plate and the surrounding gas. The conduction correction factor K_{cond} is obtained from the calibration processes. The value of K_{cond} varies depending on different application conditions of PT. For example, if the back side of PT is exposed to the surrounding gas at ambient temperature and the heat loss effect is more significant, a higher value of K_{cond} is expected to have a between fitting between the measured incident heat flux using PT and that measured by commercially available water-cooled heat flux gauge. Typically, K_{cond} ranges from 5 to 22 W/m^2 K for the PT in standards for various applications [15]. Ingason's method was successful to measure the heat flux, especially in the steady state condition. However, during the beginning of the heating phase (low surrounding gas temperature environment), the incident heat flux is still underestimated somewhat if Ingason's method is applied. Based on Ingason's analysis, the underestimation was most likely due to lateral conduction along the metal plate [16].

2.4.2 Haggkvist's method

Haggkvist et al. [9] stated that for the heat loss term, in reality, it should include not only the effects of conduction through the insulation to the back of PT and the in-plane conduction within the nickel alloy plate, but also the heat absorbed by the insulation when the temperature of nickel alloy plate and the insulation increases. To more comprehensively reflect this effect, Haggkvist et al. proposed the correction terms of heat loss including not only the conduction correction factor K_{cond} as shown in Eq. (9), but also the heat storage correction term of the heat flux associated with lumped heat capacity. The heat storage correction term is expressed as Eq. (10), in which a portion of the heat capacity of the insulation is added to that of nickel alloy plate of PT. This is based on an assumption of the uniform temperature distribution exists within the nickel alloy plate and part of the insulation. C_{PT} represents the effective heat capacity of the PT by considering the heat stored within the insulation when its temperature increases. The magnitudes of both K_{cond} and C_{PT} have

been obtained numerically by comparisons against a 2-D finite element model of the PT in well-defined thermal exposure conditions. Depending on different metal plates and insulation materials used to make PT, and different thermal exposure conditions, the specific values of K_{cond} and C_{PT} vary. Then this method was validated against experimental heat exposures. The results of Haggkvist's method show that form the aspect of heat flux measurement, a good agreement between the PT and the commercially available water-cooled heat flux gauge is achieved over both transient state and steady state.

$$\dot{q}''_{stored} = (c_{met}\rho_{met}d_{met} + \beta c_{ins}\rho_{ins}d_{ins})\frac{dT_{PT}}{dt} = C_{PT}\frac{dT_{PT}}{dt} \quad (10)$$

Where:

c_{met} = Specific heat of metal plate [kJ/(kg K)]

ρ_{met} = Density of metal plate (kg/m^3)

d_{met} = Thickness of metal plate (m)

β = Portion of the insulation

c_{ins} = Specific heat of insulation [kJ/(kg K)]

ρ_{ins} = Density of insulation (kg/m^3)

d_{ins} = Thickness of insulation (m)

T_{PT} = Temperature of metal plate (K)

C_{PT} = Heat storage lumped heat capacity [J/(m^2 K)]

2.4.3 Hidalgo's method

In Hidalgo's method [5], the authors used the thin-skin calorimeter (TSC) to measure incident radiation heat flux at the exposed surface of solid elements in large-scale fire tests. Basically, PT is a specific type of TSC, which simply consists of a thin metallic disc and a thick insulation core. The authors developed a new incident radiation heat flux calculation method using TSC to account

for not only the effect of conduction heat loss, but also the effect of uncertainties associated with the simplicity of the measurement technique. In the study of Hidalgo et al., it is assumed that the amount of heat loss from the metal plate to the insulation is proportional to the amount of absorbed incident incoming heat flux (from incident radiation and/or hot gases) as shown in Eq. (11). C is the temperature-dependent conduction correction factor for incident radiation heat flux calculations using TSC, which can be obtained from the calibration process.

$$\dot{q}''_{cond} = C \bullet \alpha_{disc} \bullet \dot{q}''_{inc} \tag{11}$$

Where:

C = Thin skin calorimeter correction factor

α_{disc} = Absorptivity of the thin skin calorimeter metallic disc

$\dot{q}''_{inc}$ = Incident heat flux (W/m^2)

From the calibration conducted using a Heat Transfer Rate Inducing System (H-TRIS), a clear linear trend of the conduction correction factor varying with the metallic disc temperature was identified, despite at the low incident heat flux range around 20 kW/m^2. The amount of heat loss quantified using Eq. (11) includes not only the heat conduction loss through TSC but also the heat stored within the insulation core. This method has been validated using H-TRIS to produce different types of dynamic incident radiation heat flux curves, in which it was found that this method provides a good trend of incident radiation heat flux curve measured using TSC, especially during the heating periods.

In the methods discussed earlier, to compensate the heat loss effects from the metal plate to insulation pad and in-plane heat conduction of metal plate, additional correction terms were introduced into the heat balance equation of PT using the actually measured surface temperature of PT. However, if the actually measured surface temperature of PT can be corrected to the temperature that PT should achieve in an ideal 1-D heat transfer condition or a perfect insulation

condition, respectively, the instantaneous effect of heat loss from the metal plate of PT to the insulation and the surroundings can be reflected in a more practical manner. In this correction, the considerable amount of heat loss within PT is taken into account by this ideal surface temperature of PT. Based on this hypotheses, in this study, two new calculation methods are proposed to improve the accuracy of calculation of incident heat flux using PT, especially when PT was placed in a thermal environment with the surrounding gas at ambient temperature.

CHAPTER III

DESIGN OF PT

A front and side view as well as the schematic view of the PT in this study are shown in Figure 3, which typically consists of a square Inconel Alloy 600 metal plate (25.4 mm × 25.4 mm × 0.584 mm) and two layers of insulation pad. Due to such advantages as light weight and being physically and thermally stable even when being exposed to a high temperature [17], two layers of insulation pad both are ceramic fiber board. They have the same size as the Inconel Alloy 600 metal plate, but the first layer insulation facing the metal plate is 6.35 mm thick (Kaowool® PM, product of Lynn Manufacturing, Inc.), and the second layer is 12.7 mm thick (Kaowool® M, product of Morgan Advanced Material). As a standard engineering material, the thermal-physical properties of Inconel alloy 600 are shown in Table 1. One Type-K 24-gauge (0.511 mm in diameter) TC (product of Omega Engineering) is welded to the center of the unexposed surface of Inconel Alloy 600 metal plate, which reads the front surface temperature of metal plate if lumped heat capacitance analysis is valid. Moreover, compared with the PT in standards, another TC bead (Type-K 24-gauge (0.511 mm in diameter), product of Omega Engineering) is inserted in the middle between two ceramic fiberboard layers to measure the back surface temperature of the first layer of ceramic fiberboard (T_b). With one layer of 6.35 mm thick cement board on the back acting as supporting frame, all these pieces are gently held together being wrapped by two thin metal mechanical wires as shown in Figure 3. See Appendices A for lumped heat capacitance analysis.

To prevent the metal plate of PT from significant oxidization in a high temperature, the front surface of the Inconel Alloy 600 metal plate was sprayed with a black color silicone-based high heat paint (Rust-Oleum), which can stand temperatures up to 1366 K. To achieve a relatively stable emissivity in a wide temperature range, the PT underwent a heat treatment first before being used in any application. After these treatments, the emissivity of PT is determined as a representative value of 0.85 in this study [18], [19].

Table 1. The thermal-physical properties of Inconel alloy 600.

Material	Density [kg/m^3]	Specific heat capacity [J/kg K]
Inconel alloy 600	8420	444

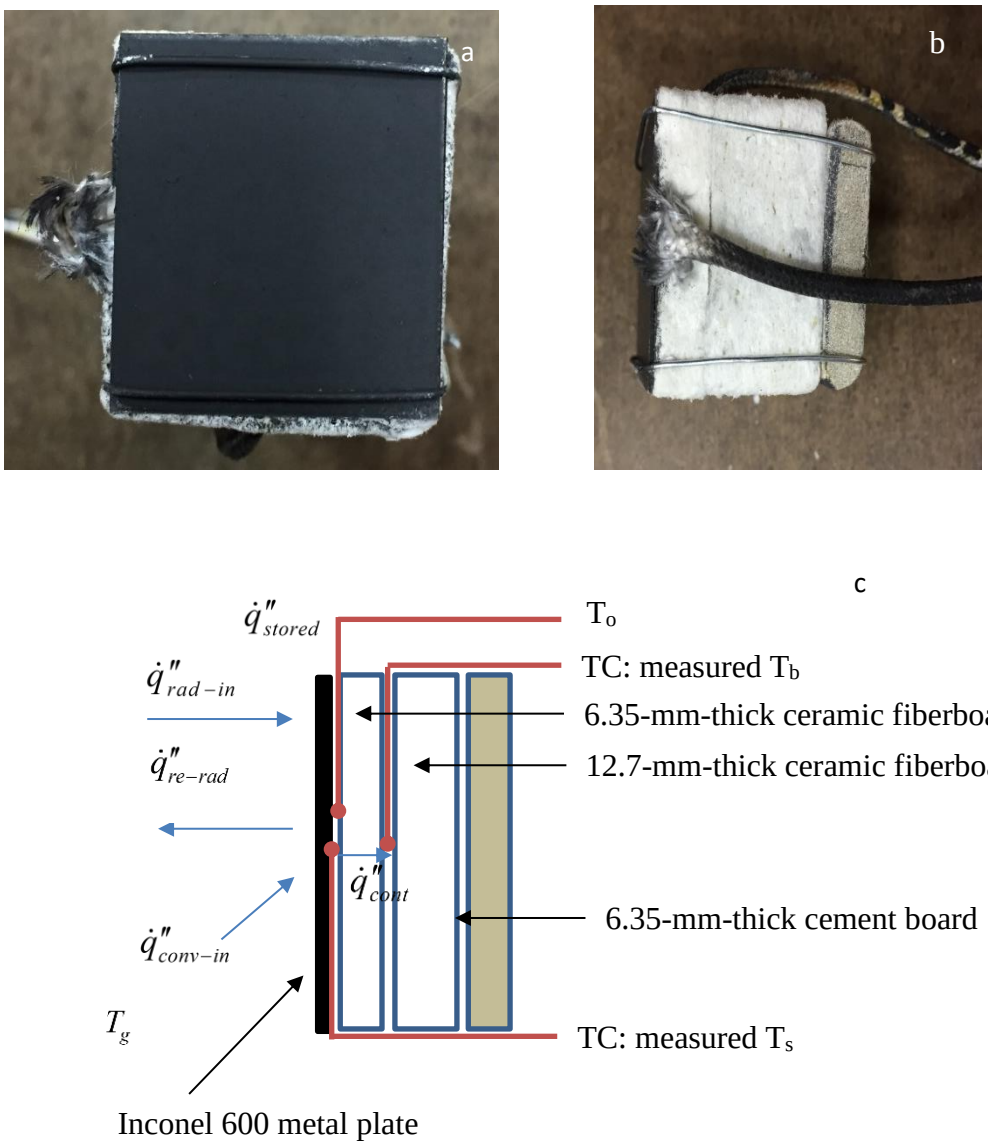

Figure 3. (a) Front view of the PT; (b) Side view of the PT; (c) A schematic view of the PT with heat balance at the surface of the PT.

Compared with the PT in standards, the new PT has a smaller exposed surface area, which is almost similar to that of typical commercially available water-cooled heat flux gauges. Additionally, the new PT is also characterized by a thinner metal plate than the PT in standards, so that the new PT can response faster when being exposed to a certain thermal environment. Based on the lumped heat capacitance analysis of the metal plate of PT, due to its low thermal mass and high thermal

conductivity, its Biot number (Bi) in a regular fire is much less than 0.1, indicating that negligible temperature gradient exists within the metal plate of PT and it is reasonable to assume a uniform temperature distribution through the metal plate [20]. This thermal behavior makes it easier to quantify the amount of heat stored within the metal plate of PT when its temperature increases. The total thickness of insulation pads of new PT is larger than that of PT in standards, which contributes to reducing the amount of heat loss from the metal plate to the insulation pad, at least in the normal direction.

The first layer of insulation pad is thinner than that of PT in standards and its thickness is smaller than its width and length. Given that, with the heat loss from the sides of PT being ignored, simply assuming 1-D heat transfer within PT from the metal plate through the insulation pads, the front surface temperature (T_0) of the first layer insulation pad in contact with the metal plate can be determined from the temperature measurement by the second TC inserted between two layers of insulation pad using the inverse heat conduction method (explicit or implicit method). With this temperature and taking the metal plate of PT as the control volume, its heat balance can be expressed as Eq. (12), which h_{cont} is the contact heat transfer coefficient between the metal plate of PT and the front surface of the first layer of ceramic fiber board.

$$\rho c_p \delta \frac{dT_s}{dt} = \varepsilon_{PT} \dot{q}''_{inc-rad} - \varepsilon \sigma T_s^4 - h(T_s - T_g) - h_{cont}(T_s - T_0) \tag{12}$$

Where:

h_{cont} = Contact correction factor (W/m^2 K)

T_0 = Temperature of the first node of ceramic fiber board (K)

Combining Eq. (12) with Eq. (5), the equivalent total heat flux is expressed as Eq. (13), which is referred as 1-D heat transfer method in this study for comparison.

$$\dot{q}''_{HFG} = \varepsilon_{HFG}\left(\frac{1}{\varepsilon_{PT}}\rho c_p \delta \frac{dT_s}{dt} - \frac{1}{\varepsilon_{PT}} h(T_g - T_s) + \frac{1}{\varepsilon_{PT}} h_{cont}(T_s - T_0) + \sigma T_s^4\right) - \varepsilon_{HFG}\sigma T_\infty^{\ 4} \qquad (13)$$

However, considering that in an ambient surrounding gas temperature condition, the amount of heat loss from the sides of PT is not negligible, which may directly lead to the underestimation of equivalent total heat flux in such a scenario. Definitely, a 3-D heat transfer model within the PT can be employed to more accurately and practically reflect the total amount of heat loss not only in the normal direction but also in lateral direction. However, a more complex system is required to do 3-D heat transfer calculation and more measurement devices are needed to determine the boundary conditions, which is not economically and technically friendly to fire engineers in a real fire test field. Faced with this challenge, the main aim of this study is to propose a new method to improve the accuracy of using PT to determine the thermal boundary conditions in an ambient surrounding gas temperature condition.

CHAPTER IV

DIFFERENT METHODS

4.1 Method 1: ideal 1-D heat transfer model

For this method, the ideal surface temperature of PT is defined as the temperature PT should achieve in an ideal 1-D heat transfer model. Compared with this ideal surface temperature, due to the inherent heat loss effect, the actually measured surface temperature of PT is lower. However, if the actually measured surface temperature of PT can be corrected to its ideal temperature, the simple 1-D heat transfer model within PT still can be employed to determine the thermal boundary condition but still with relatively high accuracy. In this case, the heat transfer between the metal plate and the first layer insulation pad can be described as Eq. (14). It should be noted that the value of T_0 depends on not only the back surface temperature of the first insulation pad (T_b) but also the temperature of the metal plate of PT.

$$\dot{q}''_{cont} = h_{cont}(T_{s-ideal} - T_0) \tag{14}$$

Where:

$\dot{q}''_{cont}$ = Contact heat loss (W/m^2)

$T_{s-ideal}$ = Ideal surface temperature of Inconel 600 metal plate (K)

When being exposed to a certain incident heat flux as shown in Eq. (15), taking the metal plate of PT as the control volume, the heat balance of PT is expressed as Eq. (16) with the term of $T_{s-ideal}$ in an ideal 1-D heat transfer model. In this equation, all the effects of heat loss from the sides of

PT are included by $T_{s-ideal}$. The correlation between the actually measured surface temperature of PT and its corresponding ideal surface temperature will be identified in the following calibration process. Additionally, if the calibration process is conducted properly, this ideal surface temperature of PT will also account the uncertainties associated with the emissivity and TC measurement error, etc.

$$\dot{q}''_{inc} = \varepsilon_{PT}\dot{q}''_{inc-rad} - h(T_s - T_g) \tag{15}$$

$$\rho c_p \delta \frac{dT_{s-ideal}}{dt} = \dot{q}''_{inc} - \varepsilon_{PT}\sigma T_{s-ideal}^4 - h_{cont}(T_{s-ideal} - T_0) \tag{16}$$

Combining Eq. (16) with Eq. (5), in an ambient surrounding gas temperature condition, the equivalent total heat flux is expressed as Eq. (17), which is referred as ideal 1-D heat transfer method in this study for comparison.

$$\dot{q}''_{HFG} = \frac{\varepsilon_{HFG}}{\varepsilon_{PT}}\left[\rho c_p \delta \frac{dT_{s-ideal}}{dt} + h(T_s - T_g) + \varepsilon_{PT}\sigma T_{s-ideal}^4 + h_{cont}(T_{s-ideal} - T_0)\right] - \varepsilon_{HFG}\sigma T_\infty^4 \tag{17}$$

4.2 Method 2: perfect insulation model

For direct engineering use, the first method still needs to use inverse heat conduction model to characterize the heat transfer within the insulation pad of PT. To further simplify this method and bring more convenience to fire engineers in real applications, another ideal surface temperature is defined as the temperature that PT should achieve in a perfect insulation condition or adiabatic condition. In this case, similarly, when being exposed to a certain incident heat flux as shown in Eq. (15), with the metal plate of PT as the control volume, the heat balance of PT is expressed as Eq. (18) with the term of $T_{s-ideal}$ in a perfect insulation model. In this equation, there is no additional heat loss term included.

$$\rho c_p \delta \frac{dT_{s-ideal}}{dt} = \varepsilon_{PT} \dot{q}''_{inc} - \varepsilon_{PT} \sigma T^4_{s-ideal} \tag{18}$$

Compared with Eq. (16), this ideal surface temperature takes into account only the heat loss from the sides of PT and the uncertainties associated with the thermos-physical properties of Inconel alloy 600 and ceramic fiberboard, but also the heat loss through the normal direction of PT. Then it is conjectured that the actual measured surface temperature of PT can be corrected to its ideal surface temperature in a perfect insulation condition, and some correlation may exist between these two temperatures although they are different. With this correlation, this adiabatic heat transfer model can be employed to determine the thermal boundary condition.

Combining Eq. (18) with Eq. (5), in an ambient surrounding gas temperature condition, the equivalent total heat flux is expressed as Eq. (19), which is referred as perfect insulation heat transfer method in this study for comparison.

$$\dot{q}''_{HFG} = \frac{\varepsilon_{HFG}}{\varepsilon_{PT}} \left[\rho c_p \delta \frac{dT_{s-ideal}}{dt} + h(T_{s-ideal} - T_g) + \varepsilon_{PT} \sigma T^4_{s-ideal} \right] - \varepsilon_{HFG} \sigma T^4_{\infty} \tag{19}$$

CHAPTER V

CONE CALORIMETER SET UP AND PT CALIBRATION PROCEDURE

The calibration of PT was conducted under a cone calorimeter heater (Fire Testing Technology Limited). In general, for the specimen tested using a cone calorimeter, it is exposed to not only the radiation heat transfer from the cone calorimeter heater, but also convection heat transfer attributed by surrounding gas. However, due to the inherent uncertainty associated with the determination of convective heat transfer coefficient using empirical or semi-empirical correlations [21], it is important to reduce the effects of convection as achievable achievably as possible, in order to improve the calibration results of PT. Keeping this intention in mind, with its smaller size compared to the PT in standards, the PT was put in a horizontal orientation under the cone calorimeter heater as shown in Figure 4, to reduce the effect of convection cooling by surrounding gas at an ambient temperature to hot PT surface [22]. During the calibration process of PT, the cone calorimeter heater was increased from ambient temperature to 300 ºC first and then to 900 ºC in the increment of 100 ºC, corresponding to a heat flux in the range from 0-75 kW/m^2. At each steady state, in order to obtain more stable temperature measurement value, PT was continuously heated for at least 300 s. For this PT calibration process in this configuration, the Rayleigh number is small enough in the order of 1000, which further approves that the effect of convection heat transfer to hot PT surface by cool surrounding gas is negligible [23]. In other words, the incident incoming heat flux is only from incident radiation heat flux.

As shown in Figure 4, the Schmidt-Boelter type water-cooled total heat flux gauge (THG) and radiometer were also installed under the cone calorimeter heater, and their heat absorption surfaces were kept at the same level as the PT. Additionally, these three devices were put as close to each other as possible (within 10 cm) and 25 mm away from the bottom of cone calorimeter heater in accordance with ISO-5660, where these three devices are exposed to the same amount of incident radiation heat flux from the cone calorimeter heater above [22]. Therefore, the value of $\dot{q}''_{inc-rad}$ in Eq. (5) is not only the incident radiation heat flux of THG but also the correctional incident radiation of PT in this configuration.

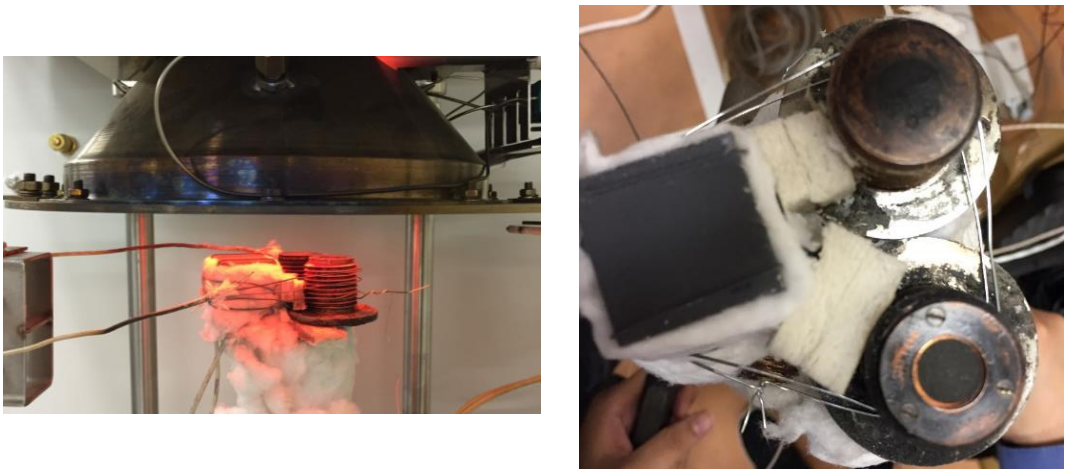

Figure 4. Configuration of calibration setup under cone calorimeter heater.

5.1 Calibration of PT for method 1

With the convective heat transfer being negligible during the calibration process, the heat balance equation of PT in steady state is written as Eq. (20), with the term of $T_{s-ideal}$ in an ideal 1-D heat transfer model.

$$0 = \varepsilon_{PT}\dot{q}''_{inc-rad} - \varepsilon_{PT}\sigma T_{s-ideal}^4 - h_{cont}(T_{s-ideal} - T_0) \quad (20)$$

With the incident radiation heat flux quantified by THG, in Eq. (19), there are still two unknown terms: $T_{s-ideal}$ and h_{cont}. Basically, the value of h_{cont} is a thermal-physical property, which depends on the surface roughness of materials in contact, the thermal properties of materials, the contact pressure, and temperature, etc. [24]. These factors directly contribute to the temperature drop between the two materials in contact. Some researchers ignored this temperature drop by assuming the perfect contact condition [2]. Considering the relatively loose structure and poor conductivity of ceramic fiber board and that the contact between the metal plate and the back insulation is not that tight in a high temperature, that temperature drop indeed exists. Although some theories have been developed to predict the thermal contact conductance, or thermal contact resistance between materials, the accurate predication is still very difficult. For this study, rather than the accurate determination of h_{cont}, a representative value of h_{cont} is necessary to reflect the instantaneous heat transfer between the metal plate of PT and the back insulation in contact.

For one heating process from ambient temperature to 900 ºC under the cone calorimeter heater as described earlier, using the actual surface temperature of PT and back surface temperature of first layer of ceramic fiberboard and assuming 1-D heat transfer in the normal direction, the amounts of $\dot{q}''_{cont}$ are quantified as shown in Figure 5 by employing different values of h_{cont} ranging from 10 to 10^4 W/m^2 K and the thermos-physical properties of ceramic fiber board as shown in Table 2. With the increase of h_{cont}, $\dot{q}''_{cont}$ increases as well as expected. However, when h_{cont} increases to a certain value, $\dot{q}''_{cont}$ approaches almost constant even with the increase of h_{cont}, which $\dot{q}''_{cont}$ is insensitive to the variation of h_{cont}. Based on this analysis, a representative value of h_{cont} is chosen as 1000 W/m^2 K to reflect the dynamic change of $\dot{q}''_{cont}$ in a transient state.

Table 2. The thermal-physical properties of first layer of ceramic fiberboard.

Material	Density [kg/m^3]	Specific heat capacity [J/kg K]	Thermal conductivity [w/m K]
Ceramic fiberboard (Kaowool® PM)	256	$0.0000000453T^3$- $0.0002677776T^2$+0.6268103151T +613.6579670929	$0.00000015233T^2$ - 0.0001185T +0.0947

The material properties of ceramic fiberboard is shown in Appendices A.

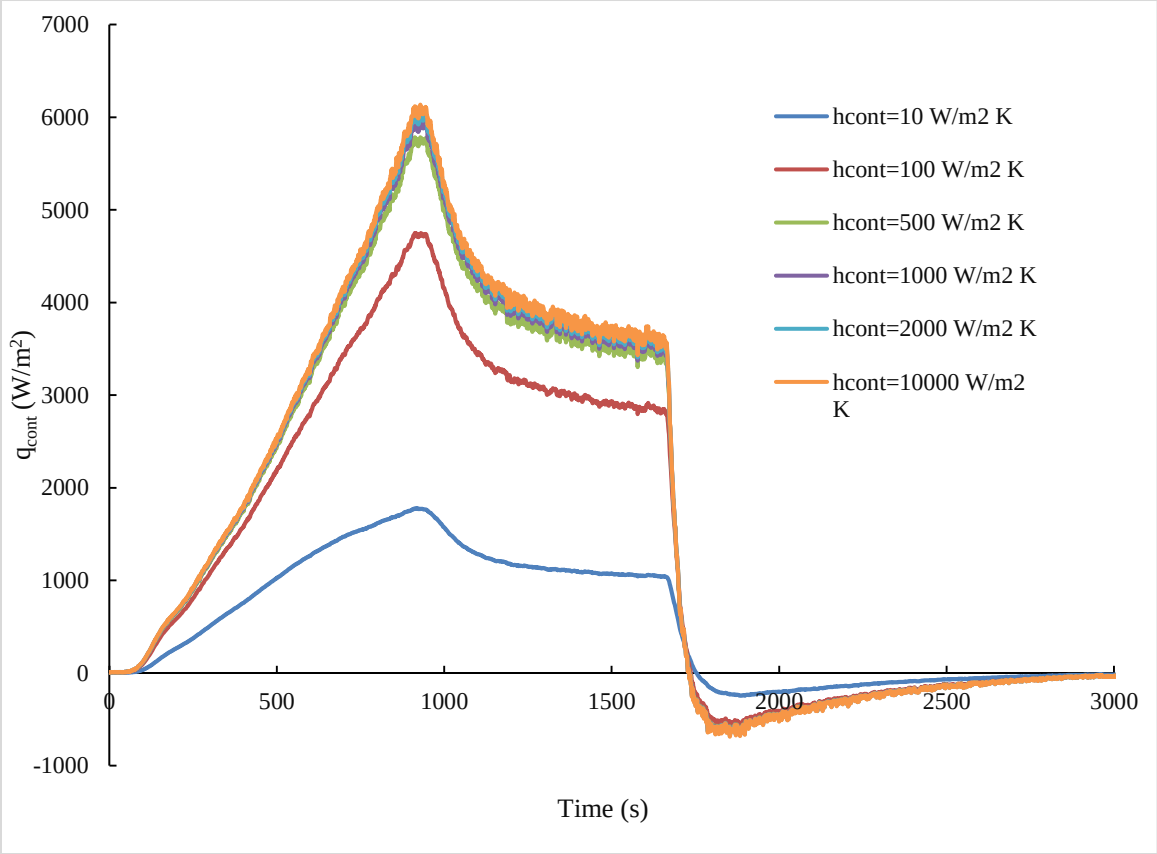

Figure 5. The variation of $\dot{q}''_{cont}$ with different values of h_{cont}.

With the determination of h_{cont}, in Eq. (20), the value of $T_{s-ideal}$ were determined subsequently. The relationship between $T_{s-ideal}$ and T_s is established as shown in Eq. (21) and Figure 6.

$$y = -0.0002799x^2 + 1.382x - 80.37 \quad (21)$$

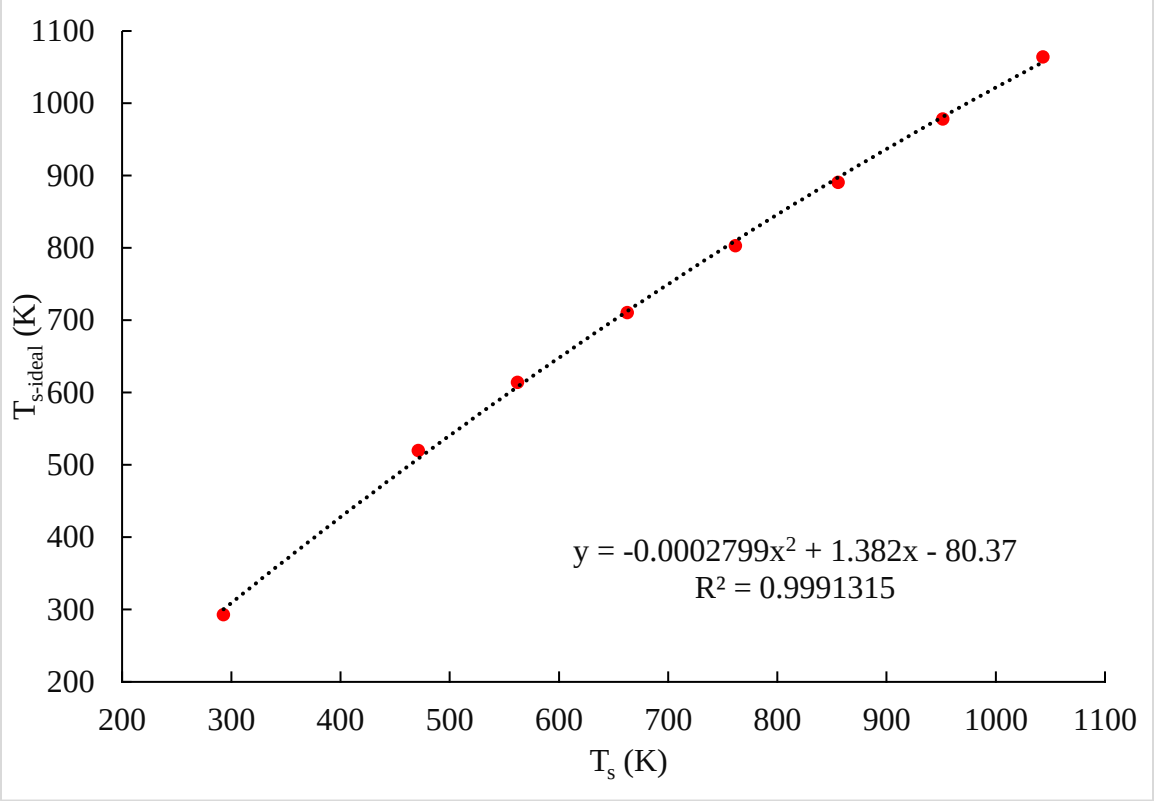

Figure 6. The correlation between $T_{s-ideal}$ and T_s for the ideal 1-D heat transfer model.

5.2 Calibration of PT for method 2

Similarly, with the convection heat transfer being negligible during the calibration process, the heat balance equation of PT in steady state is written as Eq. (22), with the term of $T_{s-ideal}$ in a perfect insulation condition.

$$0 = \varepsilon_{PT}\dot{q}''_{inc-rad} - \varepsilon_{PT}\sigma T^4_{s-ideal} \quad (22)$$

With the incident radiation heat flux quantified by THG, in Eq. (22), the corresponding value of $T_{s-ideal}$ was determined for each steady stage. The relationship between $T_{s-ideal}$ and T_s is established as shown in Eq. (23) and Figure 7.

$$y = -0.0004446x^2 + 1.607x - 124.5 \quad (23)$$

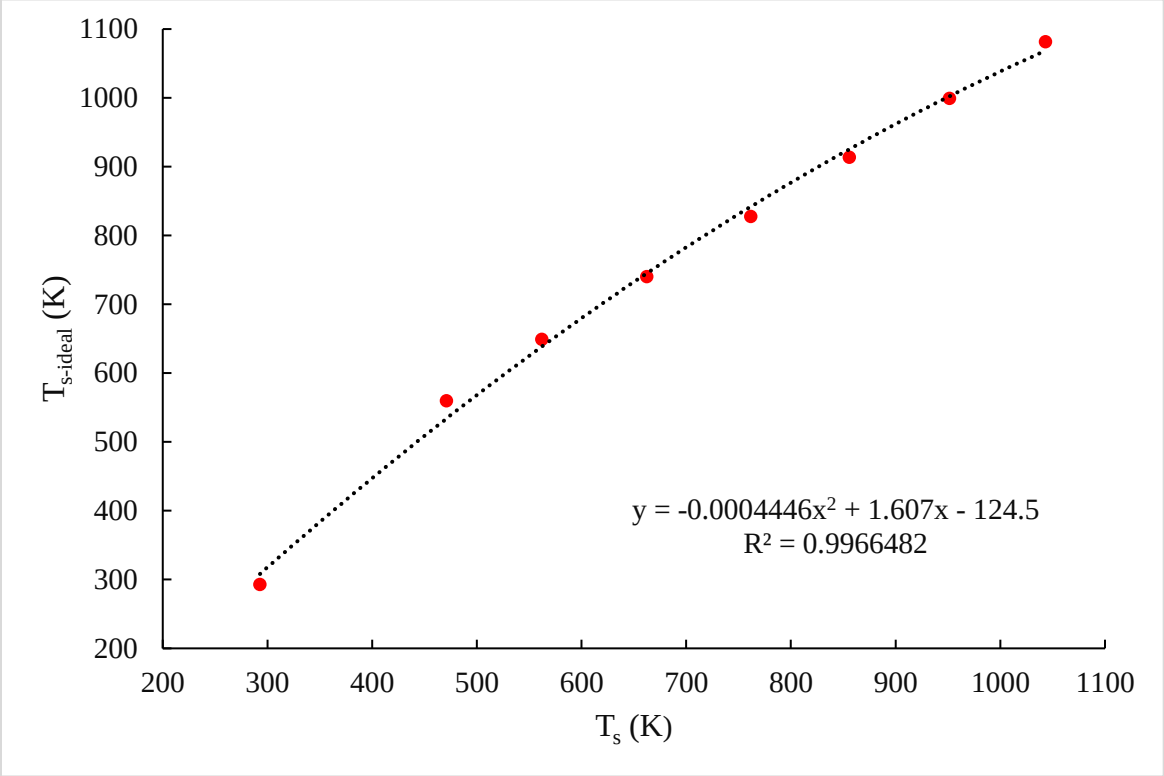

Figure 7. The correlation between $T_{s-ideal}$ and T_s for the perfect insulation model.

It should be noted that the correlations established above between $T_{s-ideal}$ and T_s are changed once the material, thickness, and size of metal plate and insulation are changed.

CHAPTER VI

VALIDATION OF THE METHODS NEWLY PROPOSED

6.1 Validation under the cone calorimeter heater

With the relationships between $T_{s-ideal}$ and T_s obtained from the calibration procedure above, the effectiveness of new methods is evaluated by comparing the equivalent total heat flux calculated using new methods with the reading of THG. As a reference, with the heat loss from the sides of PT being ignored and simply assuming 1-D heat transfer within PT, the equivalent total heat flux is also calculated using the actual temperature reading of PT. The results of the comparison are shown in Figure 8 below.

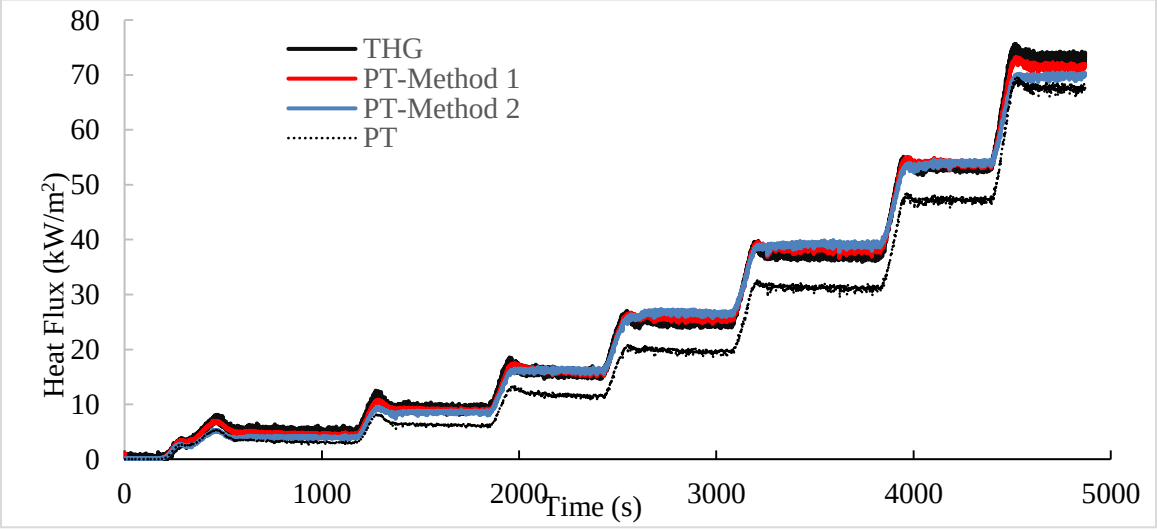

Figure 8. Comparison of equivalent total heat flux calculated using different methods under the cone calorimeter heater.

Obviously, simply assuming 1-D heat transfer within PT and only with the heat loss between metal plate and the back insulation pad in the normal direction being considered in such an ambient surrounding gas temperature condition, the equivalent total heat flux is significantly underestimated if it is directly calculated using the actual temperature reading of PT, throughout the calibration process under the cone calorimeter heater. With the method of $T_{s-ideal}$ in a perfect insulation condition, despite its simplicity, the equivalent total heat flux calculated using PT catches the general trend of heat flux variation and has a better agreement with the reading of THG. The best agreement with the reading of THG is achieved by calculating the equivalent incident heat flux using PT with the method of $T_{s-ideal}$ in an ideal 1-D heat transfer model. With this method, not only during the steady state, but also during the heating phase, the calculated equivalent total heat flux using PT matches well with that of THG, especially at low to moderate level of thermal exposure, e.g., around 50 kW/m^2. At a stronger intensity of thermal exposure, due to the high sensitivity of heat flux to temperature, if a high accuracy of equivalent total heat flux calculation using PT is needed, a more accurate calibration of PT in this level of thermal exposure is required specifically, e.g., around or higher than 70 kW/m^2.

6.1.1 Quantification of equivalent total heat flux under cone calorimeter heater

The equivalent total heat flux calculated using different methods has been quantified by introducing the statistic terms called mean square error. It measures of dispersion of a value of observation relative to the target value. In this case, the target value is the total heat flux of THG. It shows how accurate of equivalent total heat flux for transient phase using different methods under cone calorimeter. The formula of mean square error is shown in Eq. (24).

$$MSE = \sqrt{\frac{1}{N}\sum_{i=1}^{N}(Y_i - \hat{Y}_i)^2} \quad (24)$$

Where:

MSE = Mean square error

N = Total time step

Y_i = Equivalent total heat flux using different methods of PT

$\hat{Y}_i$ = Total heat flux using THG

The mean square error of equivalent total heat flux of PT using different methods are listed in Table 3. As comparing the equivalent total heat flux using method 1 and method 2 to the calculated equivalent total heat flux by directly using measured surface temperature, the results of both method 1 and method 2 are much more accurate than the result of directly using measured surface temperature. The method 1 has smallest MSE, which means it is the most accurate results for the transient phase under the cone calorimeter test.

Table 3. The mean square error of equivalent total heat flux of PT for using different methods under cone calorimeter

	MSE
Method 1	1.006
Method 2	3.004
PT	50.79

6.2 Validation in real fire condition

In order to further validate the effectiveness of the newly proposed methods, PT and THG were set up to be exposed to a real pool fire in an ambient surrounding gas temperature condition.

6.2.1. Real fire experiment setup

The configuration shown in Figure 9 is the experimental setup of a regular pool fire. The heptane was used as the fuel in a 0.5 m by 0.5 m square pan. PT and THG were mounted on a vertically orientated ceramic fiberboard and they were located as close to each other as possible to ensure that

they were exposed to the same thermal environment. The vertical plate was positioned 0.5 m away from the center of the fuel pan and along the side of the fuel pan. For this configuration, the convective heat transfer coefficient was determined using the basic equation as shown in Eq. (25), with the Nusselt number is determined using the correlation shown in Eq. (26) [21].

$$\overline{Nu} = \frac{\bar{h}L}{k} \tag{25}$$

$$\overline{Nu} = 0.680 + \frac{0.670 Ra^{1/4}}{[1+(0.492/\mathrm{Pr})^{9/16}]^{4/9}} \tag{26}$$

Where:

$\overline{Nu}$ = Nusselt number

L = Length (m)

k = Thermal conductivity (W/m $^\circ$C)

Ra = Rayleigh number

Pr = Prandtl number

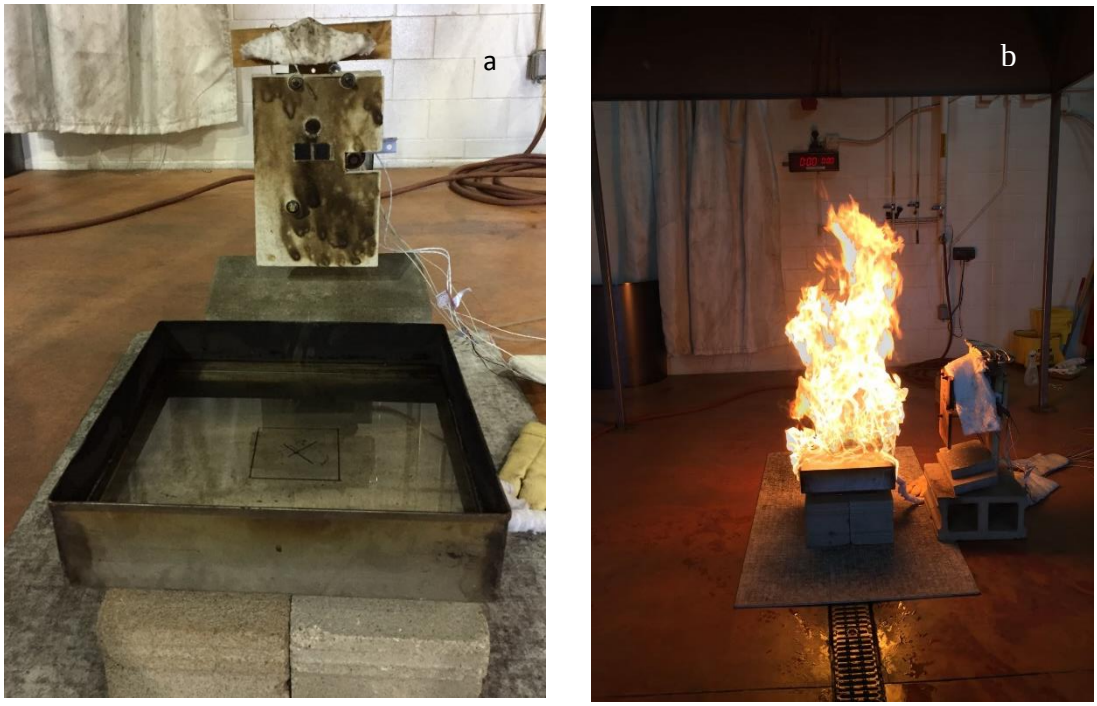

Figure 9. (a): Experimental setup of real fire to valid the new methods proposed in this study (Front view); (b): Side view.

6.2.2 Comparison of the equivalent total heat flux calculated using different methods

Figure 10 shows the equivalent total heat flux calculated using different methods for the thermal exposure from the regular pool fire. Similarly, with the lateral heat transfer within PT and the uncertainties associated with other thermo-physical factors being ignored and assuming 1-D heat transfer within PT, the equivalent total heat flux is underestimated by directly calculating it using the actual temperature of PT. With the first method proposed earlier, using $T_{s-ideal}$ in an ideal 1-D heat transfer model, the equivalent total heat flux calculated using PT has been improved, which not only catches the fast changing trend of thermal exposure from a real fire, but also matches well with the reading of THG as shown in **Figure 10**Figure 10. With the second method proposed

earlier, using $T_{s-ideal}$ in a perfect insulation model, there is still some discrepancy and underestimation between the equivalent total heat flux calculated using PT and that read by THG. However, this method still performs better the 1-D heat transfer method by ignoring the lateral heat transfer within PT and the uncertainties associated with other factors. Due to its simplicity and convenience, this method is still useful for fire engineers in real applications, but without a lot of sacrifice of accuracy.

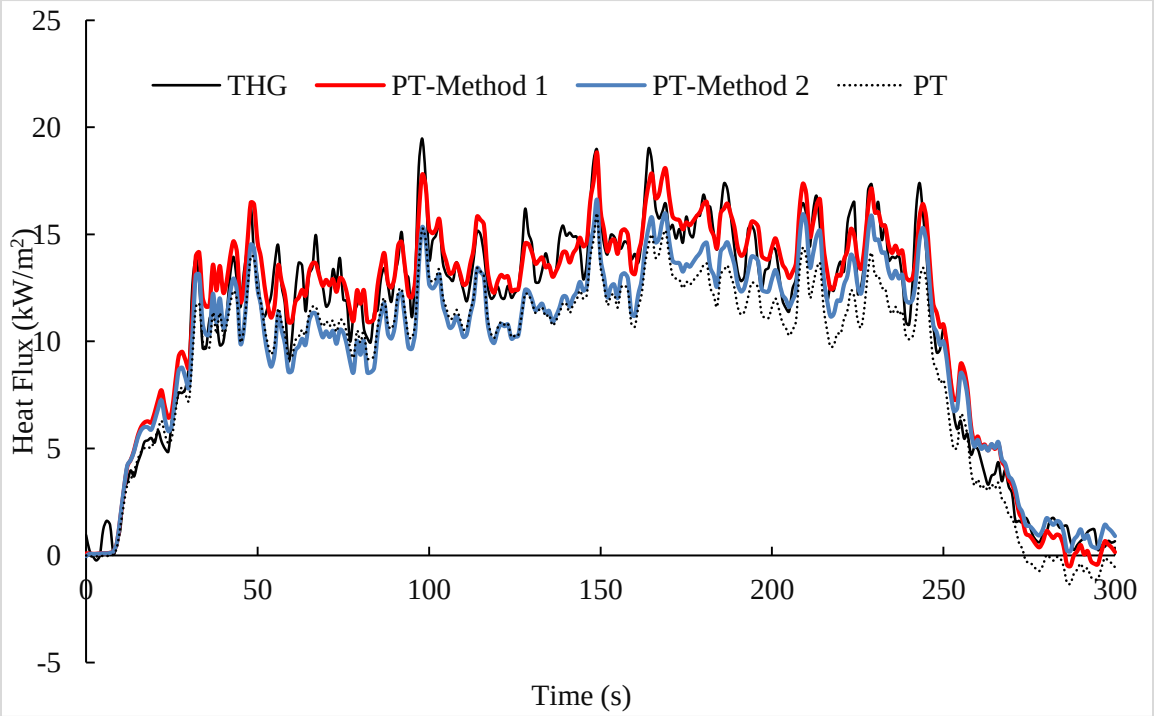

Figure 10. Comparison of the equivalent total heat flux calculated using different methods in real fire experiment.

6.2.3 Quantification of equivalent total heat flux in real fire experiment

The mean square error of equivalent total heat flux of PT in real fire experiment by using different methods are listed in Table 4. As we expect, the equivalent total heat flux using method 1 and method 2 to the calculated equivalent total heat flux by directly using measured surface temperature, the results of both method 1 and method 2 are much more accurate than the result

directly using measured surface temperature. The method 1 has smallest MSE, which means it is the most accurate results for the real fire experiment.

Table 4. **The mean square error of equivalent total heat flux of PT for using different methods in real fire experiment**

	MSE
Method 1	1.065
Method 2	2.959
PT	4.369

CHAPTER VII

CONCLUSION

This thesis presents two novel methods of calculating the equivalent total heat flux using a newly designed PT. These two methods are proposed based on the hypothesis that the actual temperature reading of PT can be corrected to an ideal surface temperature of PT to account for the uncertain factors existing to affect the accuracy of calculating the equivalent total heat flux using PT, such as heat loss, thermocouple welding, thermocouple wire heat conduction, emissivity, thermo-physical properties of insulation pad, etc. The correlations between the actual temperature reading of PT and its ideal surface temperatures were obtained from the calibration under the cone calorimeter heater for the ideal 1-D heat transfer model and the perfect insulation model, respectively. These two methods are validated against the reading of THG in a controlled thermal exposure from the cone calorimeter heater and in a real fire scenario. Generally, at a low to moderate level of thermal exposure, the accuracy of the equivalent total heat flux calculated using PT has been significantly improved by employing the ideal surface temperature of PT in an ideal 1-D heat transfer model, which has a good agreement with that read by THG. Some discrepancy is observed if simply using the ideal surface temperature of PT in a perfect insulation model to calculate the equivalent total heat flux. However, this method still shows some improvement to characterize the fast-changing trend of thermal exposure. Due to its simplicity and convenience, this method is still useful for fire engineers in real applications in the fire test field.

REFERENCES

[1] M.J. Hurley, D.T. Gottuk, J.R. Hall Jr., K. Harada, E.D. Kuligowski, M. Puchovsky, C.J. Wieczorek, *SFPE Handbook of Fire Protection Engineering*. Springer.

[2] J. Zhang and M. A. Delichatsios, "Determination of the convective heat transfer coefficient in three-dimensional inverse heat conduction problems," *Fire Safety Journal*, vol. 44, no. 5, pp. 681–690, Jul. 2009.

[3] X. Silvani and F. Morandini, "Fire spread experiments in the field: Temperature and heat fluxes measurements," *Fire Safety Journal*, vol. 44, no. 2, pp. 279–285, Feb. 2009.

[4] "ASTM E3507. Standard test method for measuring heat flux using directional flame thermometers with advanced data analysis techniques." 2015.

[5] J. P. Hidalgo, C. Maluk, A. Cowlard, C. Abecassis-Empis, M. Krajcovic, and J. L. Torero, "A Thin Skin Calorimeter (TSC) for quantifying irradiation during large-scale fire testing," *International Journal of Thermal Sciences*, vol. 112, pp. 383–394, Feb. 2017.

[6] J. Sjöström, F. Amon, G. Appel, and H. Persson, "Thermal exposure from large scale ethanol fuel pool fires," *Fire Safety Journal*, vol. 78, pp. 229–237, Nov. 2015.

[7] J. Sjöström and U. Wickström, "Different types of plate thermometers for measuring incident radiant heat flux and adiabatic surface temperature," presented at the Conference proceeding Interflam 2013 13th international Fire Science & Engingeering Conference 2013, 2013.

[8] J. Sjöström and P. Andersson, "thermal exposure from burning leaks on LNG hoses: experimental results," p. 87

[9] A. Häggkvist, J. Sjöström, and U. Wickström, “Using plate thermometer measurements to calculate incident heat radiation,” *Journal of Fire Sciences*, vol. 31, no. 2, pp. 166–177, Mar. 2013.

[10] H. Ingason and U. Wickström, “Measuring incident radiant heat flux using the plate thermometer,” *Fire Safety Journal*, vol. 42, no. 2, pp. 161–166, Mar. 2007.

[11] U. Wickström, “The plate thermometer - a simple instrument for reaching harmonized fire resistance tests,” *Fire Technol*, vol. 30, no. 2, pp. 195–208, May 1994.

[12] SBG01 manual v1722.

[13] ISO 834-11:2014 - Fire resistance tests -- Elements of building construction -- Part 11: Specific requirements for the assessment of fire protection to structural steel elements. [Online]. Available: https://www.iso.org/standard/57595.html. [Accessed: 26-May-2018].

[14] BS EN 1363-1:1999 - Fire resistance tests. General requirements. [Online]. Available: https://shop.bsigroup.com/ProductDetail/?pid=000000000019969914. [Accessed: 26-May-2018].

[15] P. S. Cumber, “Measuring Radiation Heat Fluxes from a Jet Fire Using a Lumped Capacitance Model,” *Fire Technol*, vol. 47, no. 3, pp. 665–685, Jul. 2011.

[16] C. S. Lam and E. J. Weckman, “Steady-state heat flux measurements in radiative and mixed radiative–convective environments,” *Fire and Materials*, vol. 33, no. 7, pp. 303–321.

[17] R. J. Zhang Zuotai, L. Liu, and X. Wang, “Numerical modeling and experimental study of heat transfer in ceramic fiberboard,” *Textile Research Journal*, vol. 84, no. 4, pp. 411–421, Mar. 2014.

[18] “Characterization of Pyromark 2500 Paint for High-Temperature Solar Receivers | Journal of Solar Energy Engineering | ASME DC.” [Online]. Available: https://solarenergyengineering.asmedigitalcollection.asme.org/article.aspx?articleID=1718674. [Accessed: 04-Feb-2019].

[19] R. Brandt, C. Bird, and G. Neuer, “Emissivity reference paints for high temperature applications,” *Measurement*, vol. 41, no. 7, pp. 731–736, Aug. 2008.

[20] Fundamentals of heat and mass transfer.

[21] J. Holman, *heat transfer*, 10 th. McGrwa Hill, 2010.

[22] V. Babrauskas, “Development of the cone calorimeter—A bench-scale heat release rate apparatus based on oxygen consumption,” *Fire and Materials*, vol. 8, no. 2, pp. 81–95, Jun. 1984.

[23] K. G. T. Hollands, G. D. Raithby, and L. Konicek, “Correlation equations for free convection heat transfer in horizontal layers of air and water,” *International Journal of Heat and Mass Transfer*, vol. 18, no. 7, pp. 879–884, Jul. 1975.

[24] M. G. Cooper, B. B. Mikic, and M. M. Yovanovich, “Thermal contact conductance,” *International Journal of Heat and Mass Transfer*, vol. 12, no. 3, pp. 279–300, Mar. 1969.

APPENDICES

APPENDICES A

The lumped capacitance analysis is to solve transient heating and cooling problems in the simplest and most convenient way. Hence it is important to determine under what conditions it may be used with reasonable accuracy. Based on the lumped analysis from Fundamentals of Heat and Mass Transfer textbook, the Biot number is the most significant steps. If the following condition is satisfied Bi <0.1, the error associated with using the lumped capacitance method is small.

The following analysis is based on the material properties and experiment situation.

Assume $h_c \approx 20$ W/ m^2 K, k=14 W/ m K at 298 K. Therefore,

$$Bi = \frac{hL}{k} = \frac{20 * 0.0005084}{14} = 0.000727 < 0.1$$

We use the same method for the lumped analysis of contact loss at the back surface,

Assume $h_{cont} \approx 1000$ W/ m^2 K, k=14 W/ m K at 298K.

$$Bi = \frac{hL}{k} = \frac{1000 * 0.0005084}{14} = 0.0363 < 0.1$$

For radiation, h_{rad} is expressed as,

$h_{rad} = \varepsilon\sigma(T_{RAD}^4 - T_s^4)/(T_{RAD} - T_s)$, where T_{RAD} is the equivalent radiation temperature and $\dot{q}''_{inc-rad} = \sigma T_{RAD}^4$. Based on our calculation, the maximum value of h_{rad} is $311\, w/m^2k$ under the highest heat flux we tested.

$$Bi = \frac{h_{RAD}L}{k} = \frac{311*0.001524}{14} = 0.0339 < 0.1$$

Therefore, based on the calculation above, the lumped thermal approximation of PT should be valid in our test ranges.

APPENDICES B

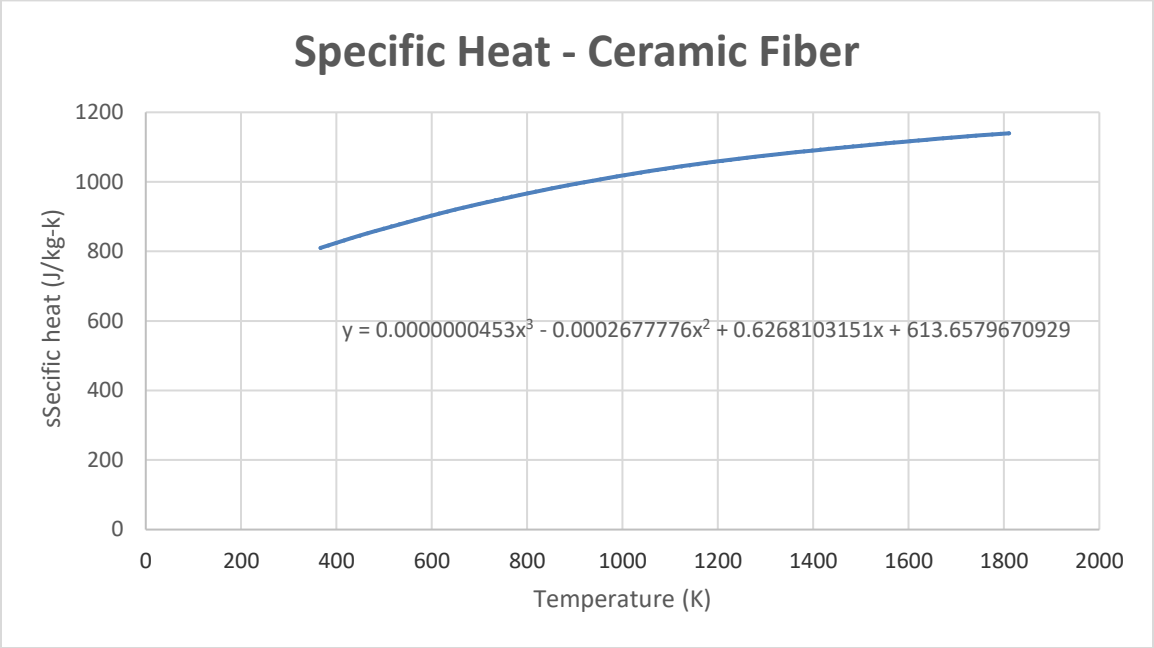

Figure 11. The specific heat (J/kg K) vs. temperature (K) for ceramic fiberboard.

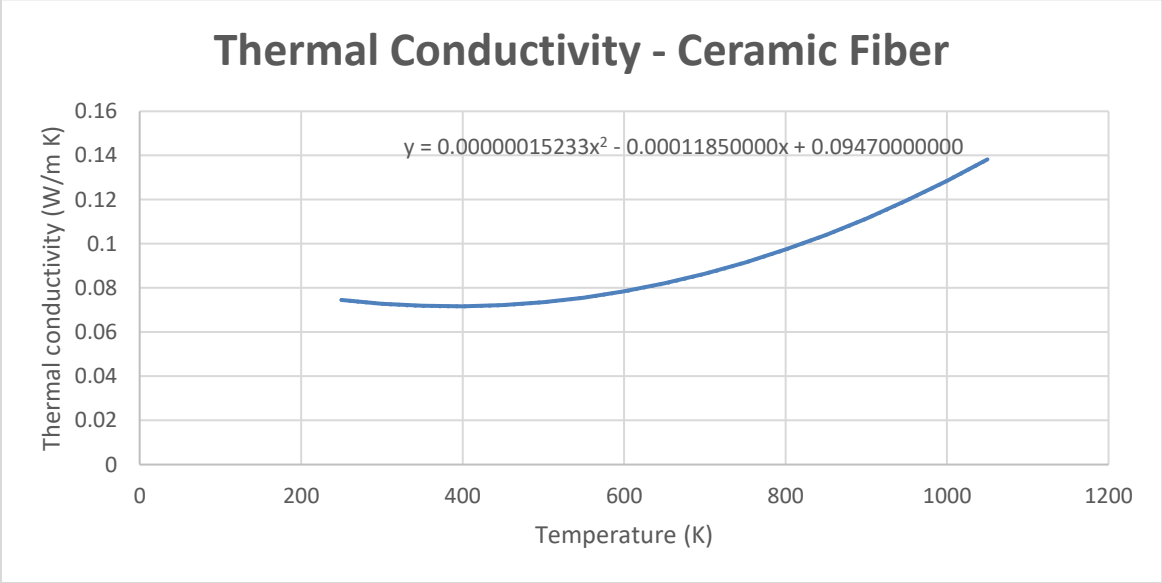

Figure 12. The thermal conductivity (W/m K) vs. temperature (K) for ceramic fiberboard.

APPENDICES C

Implicit method

The implicit method is used to

General 1-D heat conduction G.E.:

$$\frac{dT}{dt} = \frac{k}{\rho c_p}\frac{d^2T}{dx^2} \tag{1}$$

Where:

dx = Spatial node space

dt = Time node space

For spatial node,

Using Taylor series to discretize the equations for spatial nodes,

$$f_{i+1} = f_i + f_i' dx + \frac{f_i''}{2!}dx^2 + \frac{f_i'''}{3!}dx^3 + ... + \frac{f_i^n}{n!}dx^n \tag{2}$$

$$f_{i-1} = f_i - f_i' dx + \frac{f_i''}{2!}dx^2 - \frac{f_i'''}{3!}dx^3 + ... + \frac{f_i^n}{n!}dx^n \tag{3}$$

Summing Eq. (2) and Eq. (3), then rearranging the equation,

$$f_i'' = \frac{f_{i+1} - 2f_i + f_{i-1}}{dx^2} + O(dx^2) \approx \frac{f_{i+1} - 2f_i + f_{i-1}}{dx^2} \tag{4}$$

Applying Eq. (4) to temperature, so the temperature gradient is written as Eq. (5) [21],

$$\frac{d^2T}{dx^2} = \frac{T_{i+1} - 2T_i + T_{i-1}}{dx^2} \tag{5}$$

Where:

i= Spatial node

For time node,

Based on Eq. (2) and rearranging it,

$$f_i' = \frac{f_{i+1} - f_i}{dt} \tag{6}$$

Based on Eq. (3) and rearranging it,

$$-f_i' = \frac{f_{i-1} - f_i}{dt} \tag{7}$$

Based on Eq. (7) we can get f_{i+1}' [21],

$$\begin{aligned} -f_{i+1}' &= \frac{f_i - f_{i+1}}{dt} \\ \Rightarrow f_{i+1}' &= \frac{f_{i+1} - f_i}{dt} \end{aligned} \tag{8}$$

Applying Eq. (8) to temperature,

$$T_{j+1}' = \frac{T_{j+1} - T_j}{dt} \tag{9}$$

Where:

j=Time node

Based on the book of Heat Transfer, if we combine spatial node (Eq. (5)) and time node (Eq. (9)), then we can get the temperature gradients are written as Eq. (10) and Eq. (11),

$$\left(\frac{dT}{dt}\right)_{(i,j+1)} = \frac{T_i^{j+1} - T_i^j}{dt} \tag{10}$$

And,

$$\left(\frac{d^2T}{dx^2}\right)_{(i,j+1)} = \frac{T_{i+1}^{j+1} - 2T_i^{j+1} + T_{i-1}^{j+1}}{dx^2} \tag{11}$$

Applying Eq. (10) and Eq. (11) to Eq. (1), then we can get,

$$\frac{T_i^{j+1} - T_i^j}{dt} = \frac{k}{\rho c_p} \frac{T_{i+1}^{j+1} - 2T_i^{j+1} + T_{i-1}^{j+1}}{dx^2} \tag{12}$$

Rearranging Eq. (12),

$$T_i^{j+1} - T_i^j = \frac{k}{\rho c_p} \frac{dt}{dx^2} (T_{i+1}^{j+1} - 2T_i^{j+1} + T_{i-1}^{j+1}) \tag{13}$$

The value of interest is T_i^j. Therefore, rearranging Eq. (13), T_i^j can be calculated,

$$T_i^j = -\frac{k}{\rho c_p}\frac{dt}{dx^2}T_{i-1}^{j+1} + (2\frac{k}{\rho c_p}\frac{dt}{dx^2}+1)T_i^{j+1} - \frac{k}{\rho c_p}\frac{dt}{dx^2}T_{i+1}^{j+1} \quad (14)$$

Therefore, if we want to know the temperature at this time step and this spatial node for example, T_1^1, we need to know the temperature of last spatial node (T_0^2), this spatial node (T_1^2), and the next spatial node (T_2^2) at the next time step.

The followings show how to calculate these value using implicit method.

The figure below shows the spatial node of the first layer of ceramic fiberboard, and the thickness is 6.35 mm.

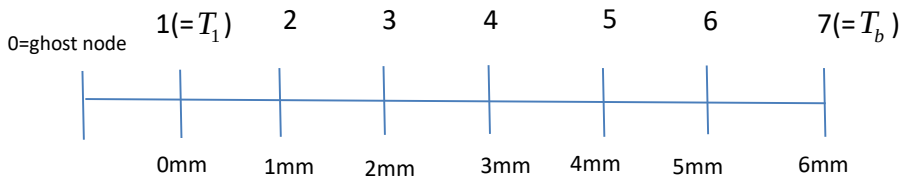

At node 7, $T_7 = T_b$ (the back surface temperature of the first layer of ceramic fiberboard) is the measured value.

If T_1 can be calculated, then we can get q''_{cont},

$$\dot{q}''_{cont} = -k\frac{dT}{dx} = k\frac{T_0 - T_2}{2dx}$$
$$\Rightarrow h_{cont}(T_s - T_1) \quad (15)$$

Therefore,

$$k\frac{T_0 - T_2}{2dx} = h_{cont}(T_s - T_1) \quad (16)$$

From Eq. (14), we can get T_1^j,

$$T_1^j = -\frac{k}{\rho c_p}\frac{dt}{dx^2}T_0^{j+1} + (2\frac{k}{\rho c_p}\frac{dt}{dx^2}+1)T_1^{j+1} - \frac{k}{\rho c_p}\frac{dt}{dx^2}T_2^{j+1} \quad (17)$$

Because T_0^{j+1} is the ghost value, we want to replace T_0^{j+1}.

If we apply time node to Eq. (16), then we can get,

$$k\frac{T_0^{j+1}-T_2^{j+1}}{2dx}=h_{cont}(T_s^{j+1}-T_1^{j+1}) \tag{18}$$

For simplified, we assume $\frac{k}{\rho c_p}\frac{dt}{dx^2}=m$,

The general equation Eq. (14) becomes,

$$T_i^j=-mT_{i-1}^{j+1}+(2m+1)T_i^{j+1}-mT_{i+1}^{j+1} \tag{19}$$

Eq. (17) becomes,

$$T_1^j=-mT_0^{j+1}+(2m+1)T_1^{j+1}-mT_2^{j+1} \tag{20}$$

Rearranging Eq. (18), we can get T_0^{j+1},

$$T_0^{j+1}=\frac{2dx}{k}h_{cont}(T_s^{j+1}-T_1^{j+1})+T_2^{j+1} \tag{21}$$

We replace T_0^{j+1} with T_s^{j+1}, T_1^{j+1}, and T_2^{j+1}.

If we apply Eq. (21) to Eq. (17), we can get

$$T_1^j=-\frac{k}{\rho c_p}\frac{dt}{dx^2}(\frac{2dx}{k}h_{cont}(T_s^{j+1}-T_1^{j+1})+T_2^{j+1})+(2\frac{k}{\rho c_p}\frac{dt}{dx^2}+1)T_1^{j+1}-\frac{k}{\rho c_p}\frac{dt}{dx^2}T_2^{j+1} \tag{22}$$

Rearranging Eq. (22), we can get T_1^j,

$$T_1^j=-\frac{k}{\rho c_p}\frac{dt}{dx^2}\frac{2dx}{k}h_{cont}T_s^{j+1}+\frac{k}{\rho c_p}\frac{dt}{dx^2}\frac{2dx}{k}h_{cont}T_1^{j+1}-\frac{k}{\rho c_p}\frac{dt}{dx^2}T_2^{j+1}+(2\frac{k}{\rho c_p}\frac{dt}{dx^2}+1)T_1^{j+1}-\frac{k}{\rho c_p}\frac{dt}{dx^2}T_2^{j+1} \tag{23}$$

T_1^j is the value of interest. In Eq. (23), the only unknow value is T_2^{j+1}. Therefore, the next step is to calculate T_2^{j+1}. T_2^{j+1} can be calculated based on T_b^{j+1} which is the back surface temperature of the first layer of ceramic fiberboard and it is the measured value. The calculation steps are shown below.

Applying Eq. (21) to Eq. (20),

$$T_1^j = -m(\frac{2dx}{k}h_{cont}(T_s^{j+1} - T_1^{j+1}) + T_2^{j+1}) + (2m+1)T_1^{j+1} - mT_2^{j+1} \quad (24)$$

Rearranging Eq. (24),

$$(m\frac{2dx}{k}h_{cont} + 2m + 1)T_1^{j+1} - 2mT_2^{j+1} = T_1^j + m\frac{2dx}{k}h_{cont}T_s^{j+1} \quad (25)$$

At node 7,

$$T_7^{j+1} = T_b^{j+1} \quad (26)$$

If we rewriting Eq. (25) for node 1, Eq. (19) for node 2, 3, 4, 5, and 6, and Eq. (26) for node 7 in a matric form,

At node 1: $(m\frac{2dx}{k}h_{cont} + 2m + 1)T_1^{j+1} - 2mT_2^{j+1} = T_1^j + m\frac{2dx}{k}h_{cont}T_s^{j+1}$ (27)

At node 2: $-mT_1^{j+1} + (2m+1)T_2^{j+1} - mT_3^{j+1} = T_2^j$ (28)

At node 3: $-mT_2^{j+1} + (2m+1)T_3^{j+1} - mT_4^{j+1} = T_3^j$ (29)

At node 4: $-mT_3^{j+1} + (2m+1)T_4^{j+1} - mT_5^{j+1} = T_4^j$ (30)

At node 5: $-mT_4^{j+1} + (2m+1)T_5^{j+1} - mT_6^{j+1} = T_5^j$ (31)

At node 6: $-mT_5^{j+1} + (2m+1)T_6^{j+1} - mT_7^{j+1} = T_6^j$ (32)

Because of $T_7 = T_b$, so we can rewriting Eq. (32),

$$-mT_5^{j+1} + (2m+1)T_6^{j+1} = T_6^j + mT_b^{j+1} \quad (33)$$

The matrix form becomes,

$$\begin{bmatrix} \text{m}\frac{2dx}{k}h_{cont} + 2m + 1) & -2m & 0 & 0 & 0 & 0 \\ -m & 2m+1 & -m & 0 & 0 & 0 \\ 0 & -m & 2m+1 & -m & 0 & 0 \\ 0 & 0 & -m & 2m+1 & -m & 0 \\ 0 & 0 & 0 & -m & 2m+1 & -m \\ 0 & 0 & 0 & 0 & -m & 2m+1 \end{bmatrix} \begin{bmatrix} T_1 \\ T_2 \\ T_3 \\ T_4 \\ T_5 \\ T_6 \end{bmatrix}^{j+1} = \begin{bmatrix} T_1^j + m\frac{2dx}{k}h_{cont}T_s^{j+1} \\ T_2^j \\ T_3^j \\ T_4^j \\ T_5^j \\ T_6^j + mT_b^{j+1} \end{bmatrix}$$

T_1^j is the first node temperature of insulation at time of j, which is the value of interest. T_s^{j+1} is the back surface temperature of metal plate at the time of j+1, which is the measured value. T_2^{j+1} is the second node temperature of insulation at time of j+1, and it can be calculated based on Eq. 2.26 to Eq. 2.32.

Therefore, the target value T_1^j and $q_{cont}^{"}$ are expressed below,

$$T_1^j = -\frac{k}{\rho c_p}\frac{dt}{dx^2}\frac{2dx}{k}h_{cont}T_s^{j+1} + \frac{k}{\rho c_p}\frac{dt}{dx^2}\frac{2dx}{k}h_{cont}T_1^{j+1} - \frac{k}{\rho c_p}\frac{dt}{dx^2}T_2^{j+1} + (2\frac{k}{\rho c_p}\frac{dt}{dx^2}+1)T_1^{j+1} - \frac{k}{\rho c_p}\frac{dt}{dx^2}T_2^{j+1} \quad (34)$$

And

$$\dot{q}_{cont}^{"} = h_{cont}(T_s - T_1) \quad (35)$$

VITA

Qingtong Liu

Candidate for the Degree of

Master of Science

Thesis: DEVELOPMENT OF A NEW METHOD TO CALCULATE INCIDENT RADIANT HEAT FLUX FROM FIRE USING PLATE THERMOMETER

Major Field: Fire Safety and Explosion Protection

Biographical:

Education:

Completed the requirements for the Master of Science in Fire Safety and Explosion Protection at Oklahoma State University, Stillwater, Oklahoma in May, 2019.

Completed the requirements for the Bachelor of Science in Fire Protection and Safety Technology at Oklahoma State University, Stillwater, Oklahoma in 2017.

Experience:

Graduate Teaching Assistant at Engineering Technology, Oklahoma State University, Stillwater, Oklahoma (August, 2017- May, 2019).